Strong Green Emission from α-SiAlON Activated by Divalent Ytterbium under Blue Light Irradiation

R.-J. Xie,* N. Hirosaki, and M. Mitomo

Advanced Materials Laboratory, National Institute for Materials Science (NIMS), Namiki 1-1, Tsukuba, Ibaraki 305-0044, Japan

K. Uheda

Tokyo University of Technology, Katakura, Hachioji, Tokyo 192-0982, Japan

T. Suehiro, X. Xu, and Y. Yamamoto

Advanced Materials Laboratory, National Institute for Materials Science (NIMS), Namiki 1-1, Tsukuba, Ibaraki 305-0044, Japan

T. Sekiguchi

Nano Materials Laboratory, National Institute for Materials Science (NIMS), Namiki 1-1, Tsukuba, Ibaraki 305-0044, Japan

Received: February 2, 2005; In Final Form: March 10, 2005

This contribution reports on luminescence properties of divalent ytterbium in α-SiAlON at room temperature. Ytterbium-doped α-SiAlON powders, with the compositions of $(M_{1-2x/v}Yb_x)_{m/v}Si_{12-m-n}Al_{m+n}O_nN_{16-n}$ (M = Ca, Li, Mg, and Y, v is the valency of M, $0.002 \le x \le 0.10$, $0.5 \le m = 2n \le 3.5$), were synthesized by sintering at 1700 °C for 2 h under 0.5 MPa N_2. A single, intense, broad emission band, centered at 549 nm, is observed due to the electronic transitions from the excited state $4f^{13}5d$ to the ground state $4f^{14}$ of Yb^{2+}. The luminescence of Yb^{2+} in α-SiAlON occurs at relatively low energy, which is attributable to the large crystal field splitting and nephelauxetic effect due to the nitrogen-rich coordination of Yb^{2+}. The dependence of luminescence properties on the Yb^{2+} concentration, chemical composition, and annealing is discussed. It is suggested that this novel green phosphor could be applied in white light-emitting diodes (LEDs) when combined with a red phosphor and a blue LED.

Introduction

α-SiAlON, isostructual with α-Si_3N_4, has a solid solution composition $M_{m/v}Si_{12-(m+n)}Al_{m+n}O_nN_{16-n}$.[1−3] In its structure, $m+n$ (Si−N) bonds are replaced by m (Al−N) bonds and n (Al−O) bonds; the charge discrepancy caused by the substitution is compensated by the introduction of a "modifying" cation M including Li, Mg, Ca, Y, and most lanthanides. The *M* cations occupy the interstitial sites in the crystal lattice, and are coordinated by seven (O, N) anions at three different M−(O, N) distances.[4] Recently, Krevel et al.[5] and we[6−10] have reported interesting photoluminescence properties of α-SiAlON doped with Eu^{2+}, Ce^{3+}, Tb^{3+}, Sm^{2+}, or Pr^{3+}. Specifically, the Eu^{2+}-doped one shows a superior absorption in the spectral region between 280 and 470 nm and a broad yellow emission in the range of 550−600 nm[5−9] and therefore is expected to be used in white light-emitting diodes when coupled to a blue LED chip.[11] α-SiAlON-based oxynitride phosphors offer the following features and therefore are of technological and scientific importance: (i) strong absorption in the visible light spectral region and long wavelength emissions; (ii) flexibility in material design, since their composition varies over a broad range without changing the crystal structure; and (iii) chemical and thermal stability, as their basic structure is based on tetrahedral, either of the Si−(O, N) or Al−(O, N) type.

It is generally accepted that the rare earth ions are usually present in α-SiAlON in their trivalent state. However, thanks to the spectroscopic studies, it is known that some rare earth ions, for example Eu, Yb, and Sm, are divalent rather than trivalent in α-SiAlON.[6,12,13] It is based on the fact that the optical spectra of divalent rare earth ions, usually arising from 4f−5d electronic transitions, differ greatly from those of trivalent ions which are ascribed to 4f−4f transitions. The emission spectrum of the former is characterized by broad bands, whereas that of the latter consists of several shape lines.[14] Furthermore, the optical spectra due to the 4f−5d transitions are very sensitive to the host lattice as a result of the strong interaction of the 5d orbitals with the crystal field.

Similar to Eu^{2+} and Ce^{3+}, Yb^{2+} commonly exhibits 4f−5d fluorescence spectra since its ground state possesses the xenon closed shell plus a $4f^{14}$ configuration.[14] The observed optical spectra of Yb^{2+} are considered to arise from $4f^{14} \leftrightarrow 4f^{13}5d$ interconfigurational transitions. Compared to Eu^{2+} and Ce^{3+}, there are relatively few investigations of the spectra of Yb^{2+} in the literature. Moreover, the studies of the luminescence spectra

* Corresponding author. Dr. Rong-Jun Xie, Advanced Materials Laboratory, National Institute for Materials Science (NIMS), Namiki 1-1, Tsukuba, Ibaraki 305-0044, Japan. Telephone: +81-29-860-4312. Fax: +81-28-851-3613. Email: Xie.Rong-Jun@nims.go.jp.

10.1021/jp050580s CCC: $30.25
Published on Web 04/23/2005

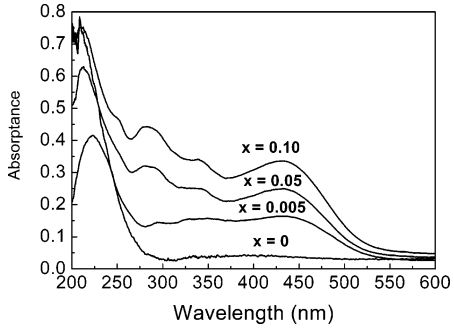

Figure 1. Diffuse reflectance spectra of Yb^{2+}-doped Ca-α-SiAlONs ($m = 2$) with varying Yb^{2+} concentrations.

of Yb^{2+} have concentrated mostly on alkaline earth halides, fluorides, sulfates, and phosphates.[15−18] In these materials the Yb^{2+} $4f^{13}5d \rightarrow 4f^{14}$ emission is between 360 and 450 nm, except 624 nm in $Ba_5(PO_4)_3Cl$ and 560 nm in $Sr_5(PO_4)_3Cl$.[15] To the best of our knowledge, there are no reports on the luminescence properties of Yb^{2+} in (oxy)nitrides. As Yb^{2+} coordinates to nitrogen in α-SiAlON and to a great extent the bonds between Yb^{2+} and (O, N) are characteristic of covalent bonding, the spectra of Yb^{2+} in it may be different from what has been reported elsewhere. Therefore, it seems interesting to investigate the luminescence spectra of Yb^{2+} in this nitrogen-rich material. In this report, the excitation and emission spectra of Yb^{2+} in α-SiAlON are investigated at room temperature. The effects of the Yb^{2+} concentration, chemical composition of host crystals, and annealing on the emission efficiency are discussed, and the potential application of this luminescent material is suggested.

Experimental Section

Yb^{2+}-doped *M*-α-SiAlON samples, with the compositions of $(M_{1-2x/v}Yb_x)_{m/2}Si_{12-m-n}Al_{m+n}O_nN_{16-n}$ (M = Ca, Li, Mg, and Y, $x = 0.002-0.1$, $0.5 \le m = 2n \le 3.5$), were prepared from α-Si_3N_4 (SN-E10, Ube Industries, Japan), AlN (Tokuyama Corp., Type F, Japan), $CaCO_3$ (Kojundo Chemical Laboratory Co. Ltd., Japan), Li_2CO_3 (Kojundo Chemical Laboratory Co. Ltd., Japan), MgO (Konoshima Chemical Co. Ltd., Japan), Y_2O_3 (Shin-Etsu Chemical Co. Ltd., Japan), and Yb_2O_3 (Shin-Etsu Chemical Co. Ltd, Japan). The powder mixture was sintered at 1700 °C for 2 h under 0.5 MPa N_2.

The phase products of synthesized powders were identified by the X-ray powder diffraction (XRD), operating at 40 kV and 40 mA and using Cu Kα radiation (RINT2200, Rigaku). A step size of 0.005° 2θ was used with a scan speed of 0.5° min^{-1}. The powder morphology was investigated by a scanning electron microscopy (SEM, Hitachi S5000).

The diffuse reflectance spectrum was recorded on a UV−vis spectrophotometer with an integrating sphere (JASCO; Ubest V-560). The reflection spectrum of Spectralon diffusive white standards is used for calibration. The photoluminescence spectra were measured at room temperature using a fluorescent spectrophotometer (F-4500, Hitachi Ltd., Japan) with a 150-W Ushio xenon short arc lamp. The emission spectrum was corrected for the spectral response of a monochromator and Hamamatsu R928P photomultiplier tube by a light diffuser and tungsten lamp (Noma, 10 V, 4 A). The excitation spectrum was also corrected for the spectral distribution of the xenon lamp intensity by measuring rhodamine-B as reference.

Results and Discussion

Absorption of Yb^{2+} in α-SiAlON. Figure 1 shows the UV−visible diffuse reflectance spectra of Ca-α-SiAlON samples

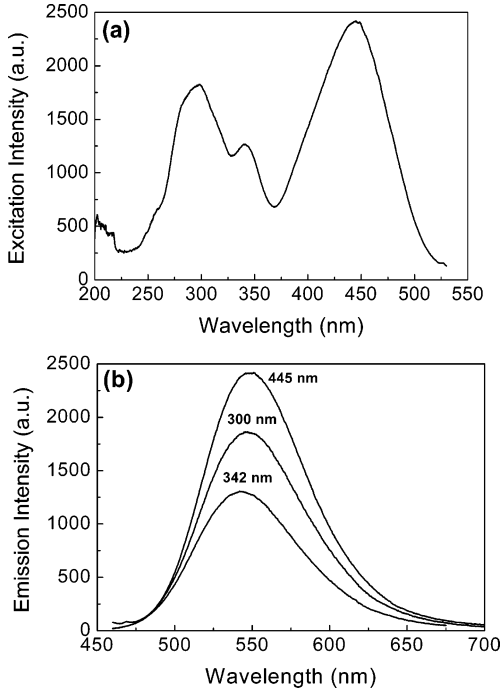

Figure 2. (a) Excitation and (b) emission spectra of the Yb^{2+}-doped Ca-α-SiAlON ($m = 2$, $x = 0.005$). The excitation spectrum was monitored at $\lambda_{em} = 549$ nm and the emission spectrum was recorded at $\lambda_{ex} = 342$, 300, and 445 nm.

doped with varying ytterbium concentration. We have reported previously that nondoped α-SiAlON is white in color and shows an absorption edge only in the UV part of the electromagnetic spectrum.[5,8,9] The ytterbium-doped α-SiAlONs, however, have several absorption bands in the UV−visible spectral region which are situated at 223, 251, 284, 300, 340, and 440 nm. The band at 223 nm is not due to the absorption of Yb^{2+} since both doped and nondoped samples have this band at the same wavelength. It must be ascribed to the absorption of the host lattice caused by charge transfer within the (Si, Al)−(O, N) network. The lanthanides are mainly trivalent, but Sm, Eu, and Yb can be reduced to divalent state and remain stable in many materials.[6,12,13,16] The visible absorption spectra of divalent lanthanides can be significantly different from those of the trivalent lanthanides. It has been observed that the $4f^n \rightarrow 4f^{n-1}5d$ transition energies for trivalent ions are in the UV spectral region, whereas for divalent ions they are within the visible region. Therefore, the absorption of ytterbium in α-SiAlON in the visible region can be clearly assigned to Yb^{2+}.

The excitation spectrum of Yb^{2+} in α-SiAlON is presented in Figure 2a. It shows clearly a number of excitation bands centered at 219, 254, 283, 307, 342, and 445 nm, respectively. These bands are consistent with those observed in the absorption spectrum. The structure in the excitation spectrum is due to the crystal field splitting of the 5d level of the Yb^{2+} ion. In contrast to the $4f^{14}$ ground state, the excited 5d level is not shielded from the ligand field, giving rise to a marked splitting of the excited level and a strong coupling to lattice vibrations. The symmetry of coordinating ligands determines the number of the split levels, whereas the ligand field strength defines the degree of splitting. The 5d level splits in a crystal field into t_2 and e levels. In an octahedral coordination of Yb^{2+}, the t_2 level is at the lower position, whereas in a tetrahedral or cubic coordination the e level is lower. The $4f^{13}$-core is coupled as in Yb^{3+} to form $^2F_{7/2}$ and $^2F_{5/2}$ states. Following the interpretation of the structure in Yb^{2+} absorption by Loh,[19] we assign the lowest peak at

TABLE 1: Approximate Energies (cm^{-1}) of $4f^{14}4f^{13}5d$ and Crystal-Field Strength of Yb^{2+}

	$4f^{13}5d$ assignments 5d		crystal-field strength
$4f^{13}$	t_{2g}	e_g	$\Delta = 10$ Dq
$^2F_{7/2}$	22,472	35,336	12,864
	29,240		
$^2F_{5/2}$	32,573	45,662	13,089
	39,370		

22 472 cm^{-1} (445 nm) as $5d(t_{2g})4f^{13}(^2F_{7/2})$ and the peak at 32 573 cm^{-1} (307 nm) as $5d(t_{2g})4f^{13}(^2F_{5/2})$; their energy difference, 10 101 cm^{-1}, is close to that of $^2F_{5/2} - {}^2F_{7/2}$.[20] Similarly, the band with maximum at 29 240 cm^{-1} (342 nm) and the shoulder at 39 370 cm^{-1} (254 nm) are assigned as $5d(t_{2g})4f^{13}(^2F_{7/2})$ and $5d(t_{2g})4f^{13}(^2F_{5/2})$, respectively; the energy difference between them is again equal to 10,130 cm^{-1} ($\approx {}^2F_{5/2} - {}^2F_{7/2}$). The should at 35 336 cm^{-1} (283 nm) and the peak at 45 662 cm^{-1} (219 nm) are assigned to $5d(e_g)4f^{13}(^2F_{7/2})$ and $5d(e_g)4f^{13}(^2F_{5/2})$, respectively, with the separation of 10,326 cm^{-1} ($\approx {}^2F_{5/2} - {}^2F_{7/2}$). The splitting between the t_2 and e level, defined as $\Delta =$ 10 Dq, is about 12 864−13 089 cm^{-1}, as shown in Table 1.

Emission of Yb^{2+} in α-SiAlON. The Yb^{2+}-doped Ca-α-SiAlON exhibits an intense green emission, as seen in Figure 2b. The emission spectrum consists of a single broadband with a maximum at 549 nm, which can be ascribed to the transition between the allowed $4f^{13}5d$ and $4f^{14}$ configurations of the Yb^{2+} ion. The strongest emission is obtained under the blue light excitation ($\lambda_{ex} = 445$ nm); no significant change of the emission profile is seen upon varying the excitation wavelength except the emission intensity. It indicates that there is only one kind of Yb^{2+} site in α-SiAlON. A rough estimate of the Stokes shift can be made by assuming that the excitation band is the mirror image of the emission band. In this way, the Stokes shift is calculated as 4300 cm^{-1}.

Both indirect and direct excitations are responsible for the emission of Yb^{2+} in α-SiAlON, but the Yb^{2+} emission obtained by the direction excitation is more efficient than that obtained by the indirect excitation, which is in good agreement with Eu^{2+} in α-SiAlON.[9] The excitation and emission mechanism of Yb^{2+} in α-SiAlON resembles that of Eu^{2+}, as explained in the following. The Yb^{2+} in the ground state is excited by the observed excitation bands into the $4f^{13}5d$ manifold which is partially located in the conduction band of the host crystal. After nonradiative relaxation with the 5d levels, a radiative transition from the excited state to the ground state takes place and results in the green emission at 549 nm. On the other hand, once excited to higher 5d levels, Yb^{2+} will auto-ionize and the excited electrons delocalize into the conduction band. Recombination with a deeply trapped hole at a defect state will proceed radiationless and does not yield luminescence.

There is not much doubt that the emission of Yb^{2+} in α-SiAlON is at a longer wavelength than normally observed (360−450 nm). Obviously, this long-wavelength emission is attributable to a low-energy position of the excited-state rather than a sizable Stokes shift. The position of the lowest $4f^{13}5d$ state with respect to the conduction band depends on many factors such as crystal field splitting, band gap and covalency. Compared to Yb^{2+} in halides, fluorides, or oxides, the ligand field around Yb^{2+} in oxynitride is stronger because of the larger effective charges of N^{3-}, thereby leading to a larger 5d splitting. The large crystal field splitting is also observed for Ce^{3+} in Y−Si−O−N oxynitrides[21] and Ce^{3+} or Eu^{2+} in α-SiAlON.[5−7] In addition, Yb^{2+} is seven-fold coordinated to (O, N) anions in α-SiAlON and the average bond length between Yb^{2+} and ligand is about 2.61 Å.[4] These Yb−(O, N) bonds are believed to be more covalent than the Yb−O bonds in oxidic materials or Yb−F bonds in fluorides because of the lower electronegativity of nitrogen (3.04) compared to those of oxygen (3.50) and fluorine (4.10).[22] It therefore would cause stronger covalency or nephelauxetic effect on Yb^{2+} in oxynitride than in oxidic or fluoride compounds. The nephelauxetic effect will reduce the energy difference between the ground state and the excited state of Yb^{2+}, inducing the shift of excitation and emission bands to longer wavelengths.

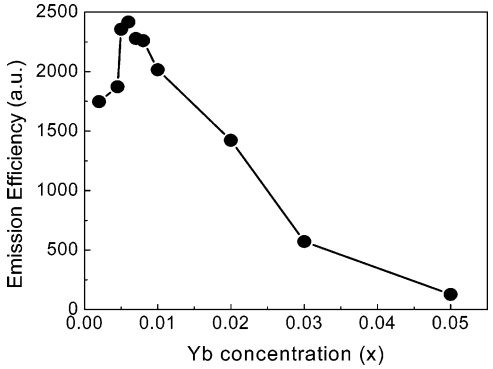

Figure 3. Concentration dependence of the emission efficiency of Yb^{2+}-doped Ca-α-SiAlONs ($m = 2$).

Concentration Quenching. The effect of the ytterbium concentration on the emission efficiency of doped Ca-α-SiAlON is shown in Figure 3. As seen, starting at a low doping level the emission efficiency rises to a maximum and falls again sharply at higher doping levels. There is no visible light emission from the sample when the Yb concentration is above $x = 0.05$. The critical concentration for concentration quenching of Yb^{2+} in Ca-α-SiAlON is $x = 0.005$. The critical concentration is an estimate for the concentration at which the percolation point is reached. The concentration quenching is more pronounced for Yb^{2+} than any other lanthanides in α-SiAlON.[9,10] Although the concentrated α-SiAlON samples absorb strongly (see in Figure 1), they do not produce efficient emission. The concentration quenching effect gives a good explanation for this observation. We have observed the red-shift of emission in Eu^{2+}- and Ce^{3+}-doped Ca-α-SiAlONs with increasing the activator concentration;[8−10] the Yb^{2+}-doped samples, however, do not show such a tendency as the Yb^{2+} concentration increases. This discrepancy is perhaps due to (i) a rather low concentration of Yb^{2+} in α-SiAlON (<5 atom %) and (ii) the equivalent ionic size of Yb^{2+} ($r_{Yb^{2+}} = 1.08$, 7CN) and Ca^{2+} ($r_{Ca^{2+}} = 1.06$, 7CN),[23] which hardly alters the chemical environment neighboring Yb^{2+}.

Compositional Dependence of the Photoluminescence Properties. The chemical composition of α-SiAlON can be altered over a wide range (defined by m and n) while the crystal structure is conserved. It thus allows for the flexibility in material design and the optimization of the luminescence properties of α-SiAlON phosphors. Figure 4 shows the luminescence efficiency of the Yb^{2+}-doped Ca-α-SiAlONs as a function of m. The Yb^{2+}-doped samples with the composition of $m = 2.0$ possess the maximal emission efficiency when the concentration of Yb^{2+} remains the same and then $x = 0.005$. This result coincides well with other rare-earth doped Ca-α-SiAlON.[10] We have stated that the compositional dependence of luminescence properties is dominantly attributed to the changes in crystallinity, phase purity, and particle morphology of α-SiAlON with varying m. With lower m values the crystallization of the powders is poor, and there are some defects in each particle which can trap or scatter the emitted light. With high m values large hard

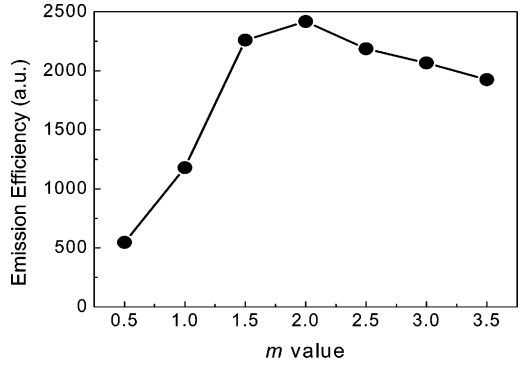

Figure 4. Compositional dependence of the emission efficiency of the Yb^{2+}-doped Ca-α-SiAlONs ($x = 0.005$).

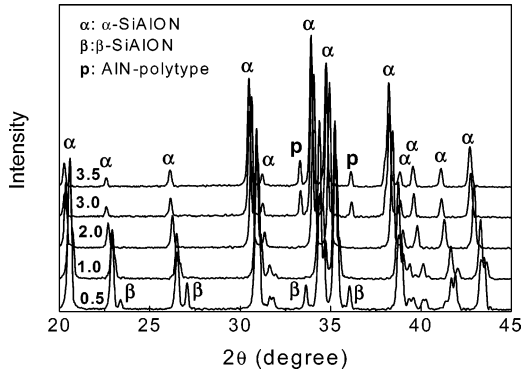

Figure 5. XRD patterns of the Yb^{2+}-doped Ca-α-SiAlONs with varying *m*. The numbers in the figure denote the *m* value. Besides the major phase of α-SiAlON, there is a secondary phase *β*-SiAlON at $m = 0.5$ and AlN-polytype at $m = 3.0$ and 3.5.

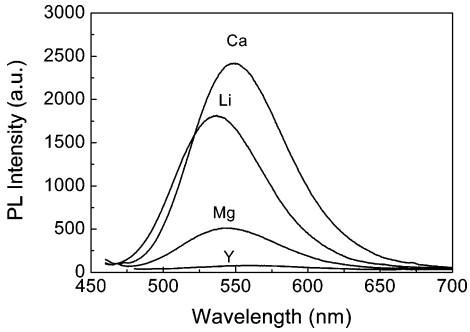

Figure 6. Effect of "modifying" cations on the emission efficiency of Yb^{2+}-doped α-SiAlONs ($m = 2$, $x = 0.005$).

agglomerates form, and this results in a low packing density of the powder which causes a strong light scattering. In addition, as seen in Figure 5, the secondary phase of *β*-SiAlON or AlN-polytype forms at low or high *m* values, respectively, which decreases the emission efficiency.

Figure 6 shows the effect of "modifying" cations on the luminescence properties of Yb^{2+}-doped α-SiAlONs. The Yb^{2+} concentration remains constant (i.e., $x = 0.005$), and the chemical composition of the host α-SiAlON is conserved as $m = 2.0$. The luminescence spectra of these α-SiAlONs strongly resemble each other, suggesting that the coordination of Yb^{2+} ions remains the same for all α-SiAlONs. The luminescence efficiency of Yb^{2+} in Ca-α-SiAlON is about 2 and 6 times higher than that of Yb^{2+} in Li- and Mg-α-SiAlON, respectively. The emission of Yb^{2+} in Y-α-SiAlON is very weak and is not visible to the naked eye. The maximal emission of Yb^{2+} in Li-, Mg-, and Ca-α-SiAlONs is situated at 537, 543, and 549 nm, respectively. The replacement of monovalent lithium ions by

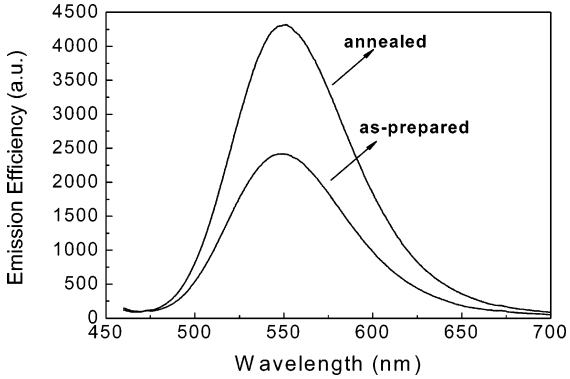

Figure 7. Effect of annealing on the emission efficiency of the Yb^{2+}-doped Ca-α-SiAlON ($m = 2$, $x = 0.005$).

divalent ytterbium requires charge compensation. Charge compensation by a nearby Li^+ vacancy or other defect will decrease the symmetry of the Yb^{2+} ion (leading to large crystal field splitting) and allow for larger relaxation in the excited state. Both effects will induce the shift of the emission to longer wavelength in Yb^{2+}-doped Li-α-SiAlON. As Mg^{2+} has a smaller ionic size than Ca^{2+}, the replacement of a smaller Mg^{2+} site will result in larger crystal field splitting and therefore lower the energy of the lowest $4f^{13}5d$ level.

Improving the Emission Efficiency by Annealing. In addition to the studying the effects of concentration and composition on the emission efficiency of the green phosphor, the effect of annealing of the phosphor was also investigated. The as-prepared powder sample ($m = 2$, $x = 0.005$) was ground and further annealed at 1700 °C for 24 h under 0.5 MPa N_2. The result is shown in Figure 7. It is clearly seen that annealing significantly increases the emission efficiency of the phosphor. The emission efficiency of the annealed powder is about 80% higher than that of the as-prepared powder. To find out the reasons for the improved efficiency, the particle morphology of the as-prepared and annealed powders is observed by a scanning electron microscopy, as shown in Figure 8. The powder morphology of the annealed sample is more regularly shaped and rodlike compared to the spherical shape of the as-prepared sample. Apparently, increasing the firing time from 2 to 24 h improves the crystallinity and increases the particle size. Figure 9 plots the ratio of absorption coefficient (*a*) and scattering coefficient (*s*) versus wavelength (200−800 nm) for the as-prepared and annealed samples. The *a/s* ratio was determined by the Kubelka−Munk equation: $a/s = (1 - R)^2/2R$ where *R* is the reflectance of both samples. As seen, the annealed sample shows a larger *a/s* ratio. Assuming the same *a* in both samples, the enhanced absorption in the annealed sample can be ascribed to a smaller scattering coefficient caused by the larger particle size. Consequently, both a better crystallinity and larger particle size account for the improved emission efficiency after annealing.

Figure 10 shows the CIE (Commission International del'Eclairge) 1931 chromatic coordinations of Yb^{2+}-doped Ca-α-SiAlON ($X = 0.323$, $Y = 0.601$). For comparison, the chromatic coordinations of commercially available green phosphors $(Ba,Mg)Al_{10}O_{17}$ (BAM):Eu^{2+}, Mn^{2+}, and ZnS:Cu, Al for white LEDs are also included. It is seen that the Ca-α-SiAlON:Yb^{2+} phosphor shows better color saturation than BAM:Eu^{2+}, Mn^{2+}, and has the coordinates close to ZnS:Cu, Al. The sulfide phosphor, however, has a poor chemical stability against moisture. The Ca-α-SiAlON:Yb^{2+} phosphor emits efficiently at the excitation wavelengths of 450−470 nm at which blue LEDs usually work, it is hence suggested that it can be used

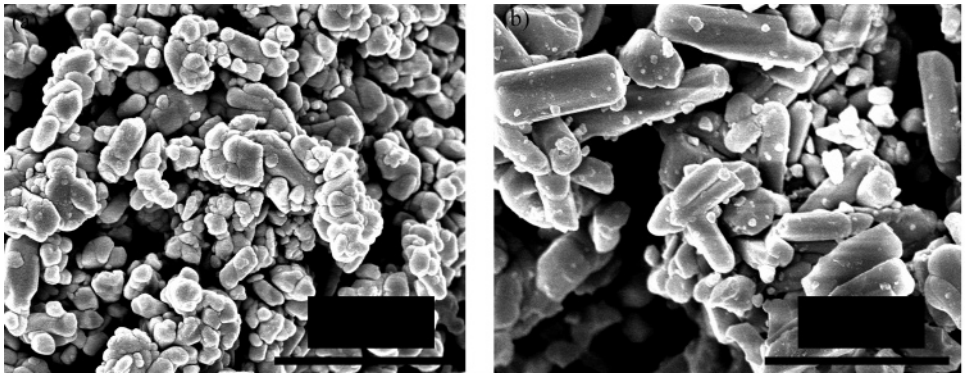

Figure 8. Scanning electron microscopy (SEM) images of the as-prepared (a) and annealed (b) samples with $m = 2$ and $x = 0.005$.

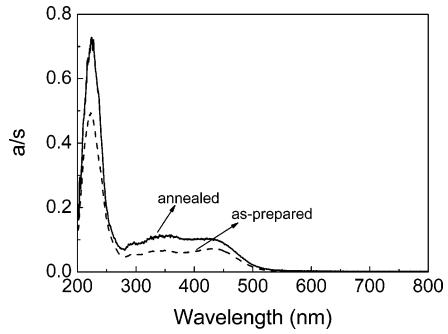

Figure 9. Diffuse reflectance spectra of the as-prepared and annealed samples. The spectra were transformed by the Kubelka−Munk equation ($a/s = (1 - R)^2/2R$, where a, s, and R are absorption coefficient, scattering coefficient, and reflectance, respectively).

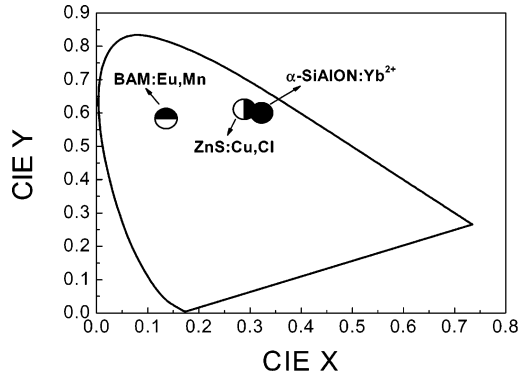

Figure 10. CIE chromatic coordinations of Ca-α-SiAlON:0.005Yb^{2+} and commercially available green phosphors BAM:Eu^{2+}, Mn^{2+}, and ZnS:Cu, Al. It indicates that the green Ca-α-SiAlON:Yb^{2+} phosphor can be used for white LEDs.

for white LEDs to create white light when combined with another red phosphor and a blue LED chip.

Conclusions

The luminescence of Yb^{2+} in α-SiAlON is characterized by the shift of the absorption from UV to the visible spectral region and an intense green emission band centered at 549 nm. The luminescence occurring at such low energies can principally be ascribed to the large crystal field splitting and nephelauxetic effect as a result of the nitrogen-rich coordination of Yb^{2+} in α-SiAlON. The luminescence properties of Yb^{2+} are greatly dependent on the activator concentration and the chemical composition of the host lattice. Annealing significantly improves the emission efficiency of the phosphor. This novel Ca-α-SiAlON:Yb green phosphor is expected to be used for phosphor-converted white LEDs.

References and Notes

(1) Hampshire, S.; Park, H. K.; Thompson, D. P.; Jack, K. H. *Nature (London)* **1978**, *274*, 31.
(2) Cao, G. Z.; Metselaar, R. *Chem. Mater*. **1991**, *3*, 242.
(3) Ekstrom, T.; Nygren, M. *J. Am. Ceram. Soc*. **1992**, *75*, 259.
(4) Izumi, F.; Mitomo, M.; Suzuki, J. *J. Mater. Sci. Lett*. **1982**, *1*, 533.
(5) Krevel, J. W. H.; Rutten, J. W. T.; Mandal, H.; Hintzen, H. T.; Metselaar, R. *J. Solid State Chem*. **2002**, *165*, 19.
(6) Xie, R.-J.; Mitomo, M.; Uheda, K.; Xu, F.-F.; Akimune, Y. *J. Am. Ceram. Soc*. **2002**, *85*, 1229.
(7) Xie, R.-J.; Hirosaki, N.; Mitomo, M.; Yamamoto, Y.; Ohashi, N. *J. Am. Ceram. Soc.* **2004**, *87*, 1368.
(8) Xie, R.-J.; Hirosaki, N.; Sakuma, K.; Yamamoto, Y.; Mitomo, M. *Appl. Phys. Lett.* **2004**, *84*, 5404.
(9) Xie, R.-J.; Hirosaki, N.; Mitomo, M.; Yamamoto, Y.; Suehiro, T.; Sakuma, K. *J. Phys. Chem. B* **2004**, *108*, 12027.
(10) Xie, R.-J.; Hirosaki, N.; Yamamoto, Y.; Suehiro, T.; Xu, X.; Mitomo, M. Unpublished.
(11) Sakuma, K.; Omichi, K.; Kimura, N.; Ohashi, M.; Tanaka, D.; Hirosaki, N.; Yamamoto, Y.; Xie, R.-J.; Suehiro, T. *Opt. Lett.* **2004**, *29*, 2001.
(12) Karunaratne, B. S. B.; Lumby, R. J.; Lewis, M. H. *J. Mater. Res.* **1996**, *11*, 2790.
(13) Shen, Z.; Nygren, M.; Halenius, U. *J. Mater. Sci. Lett.* **1997**, *16*, 263.
(14) Blasse, G.; Grabmaier, B. C. *Luminescent Materials*; Springer-Verlag: Berlin, 1994.
(15) Palilla, F. C.; O'Reilly, B. E.; Abbruscato, V. J. *J. Electrochem. Soc.* **1970**, *117*, 87.
(16) Rubio, O. J. *J. Phys. Chem. Solids* **1991**, *52*, 101.
(17) Lizzo, S.; Meijerink, A.; Blasse, G. *J. Lumin.* **1994**, *59*, 185.
(18) Lizzo, S.; Meijerink, A.; Dirksen, G. J.; Blasse, G. *J. Phys. Chem. Solids* **1995**, *56*, 959.
(19) Loh, E. *Phys. Rev.* **1969**, *184*, 348.
(20) Dieke, G. H.; Crosswhite, H. M.; Dunn, B. *J. Opt. Soc. Am.* **1961**, *51*, 820.
(21) Krevel, J. W. H.; Hintzen, H. T.; Metselaar, R.; Meijerink, A. *J. Alloys Compd.* **1998**, *268*, 272.
(22) Cotton, F. A.; Wilkinson, G. *Advanced Inorganic Chemistry*, 2nd ed.; John Willey & Sons: New York, 1966.
(23) Shannon, R. D. *Acta Crystallogr., Sect. A* **1976**, *32*, 751.